Air Oxygen Calibration of Oxygen Optodes on a Profiling Float Array

KENNETH S. JOHNSON AND JOSHUA N. PLANT

Monterey Bay Aquarium Research Institute, Moss Landing, California

STEPHEN C. RISER

School of Oceanography, University of Washington, Seattle, Washington

DENIS GILBERT

Maurice Lamontagne Institute, Fisheries and Oceans Canada, Mont-Joli, Québec, Canada

(Manuscript received 7 May 2015, in final form 20 August 2015)

ABSTRACT

Aanderaa optode sensors for dissolved oxygen show remarkable stability when deployed on profiling floats, but these sensors suffer from poor calibration because of an apparent drift during storage (storage drift). It has been suggested that measurement of oxygen in air, during the period when a profiling float is on the surface, can be used to improve sensor calibration and to determine the magnitude of sensor drift while deployed in the ocean. The effect of air calibration on oxygen measurement quality with 47 profiling floats that were equipped with Aanderaa oxygen optode sensors is assessed. Recalibrated oxygen concentration measurements were compared to Winkler oxygen titrations that were made at the float deployment stations and to the *World Ocean Atlas 2009* oxygen climatology. Recalibration of the sensor using air oxygen reduces the sensor error, defined as the difference from Winkler oxygen titrations in the mixed layer near the time of deployment, by about tenfold when compared to errors obtained with the factory calibration. The relative error of recalibrated sensors is <1% in surface waters. A total of 29 floats were deployed for time periods in excess of one year in ice-free waters. Linear changes in the percent of atmospheric oxygen reported by the sensor, relative to the oxygen partial pressure expected from the NCEP air pressure, range from −0.9% to +1.3% yr^{-1} with a mean of 0.2% ± 0.5% yr^{-1}. Given that storage drift for optode sensors is only negative, it is concluded that there is no evidence for sensor drift after they are deployed and that other processes are responsible for the linear changes.

1. Introduction

Optical oxygen sensors based on fluorescence were introduced to oceanography by Thomson et al. (1988). These sensors utilize molecular oxygen's ability to quench the fluorescence of certain lumiphores. Improved versions of these sensors have proven to be very useful devices for studying ocean ventilation (Körtzinger et al. 2004), net community production (Riser and Johnson 2008; Johnson et al. 2010), carbon export (Martz et al. 2008), gas exchange (Kihm and Körtzinger 2010), and the stability of oxygen minimum zones (Ulloa et al. 2012; Czeschel et al. 2012; Prakash et al. 2012). Most of these measurements have been made using Aanderaa optical oxygen sensors (Tengberg et al. 2006).

Despite their utility, Aanderaa optodes have a clearly recognized calibration problem (Körtzinger et al. 2005; Uchida et al. 2008; D'Asaro and McNeil 2013). Sensors are regularly seen to be significantly out of calibration, relative to the factory-supplied calibration. An analysis of 130 optodes on profiling floats found a mean error, relative to the *World Ocean Atlas 2009* (*WOA*) climatology of about

Denotes Open Access content.

Corresponding author address: Kenneth S. Johnson, MBARI, 7700 Sandholdt Road, Moss Landing, CA 95039.
E-mail: johnson@mbari.org

Publisher's Note: This article was revised on 10 December 2015 to include the open access designation that was missing when originally published.

DOI: 10.1175/JTECH-D-15-0101.1

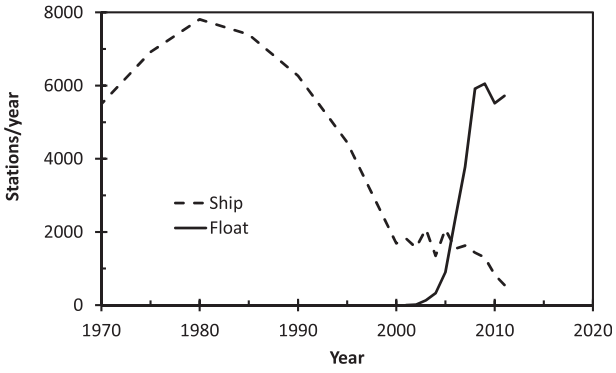

FIG. 1. Number of stations per year with oxygen samples deeper than 900 m. Data were retrieved from the World Ocean Database (Boyer et al. 2013) of the U.S. National Oceanographic Data Center (NODC). Ship data were retrieved using the ocean station data (OSD) criteria to select profiles, and float data were retrieved using the profiling float (PFL) criteria to select profiles. The search was performed for each year after 2000 and for every 5 years before 2000. No data were retrieved for years after 2011 to avoid a bias due to delays in sending data to the NODC.

$10\,\mu\text{mol kg}^{-1}$ in surface water, with sensors generally reading too low (Takeshita et al. 2013). There is, however, no significant evidence of sensor drift once these sensors are deployed in the ocean (Tengberg et al. 2006; Takeshita et al. 2013; Bittig and Körtzinger 2015). This has led to the assumption that the drift occurs primarily before deployment, a process that is termed storage drift.

The utility of oxygen sensors on profiling floats for oceanographic studies would be significantly increased if this calibration error could be minimized. For example, the number of oxygen profiles made by shipboard hydrocasts that extend to a depth of at least 900 m, and that have been included in the World Ocean Database (Boyer et al. 2013), has decreased dramatically in the past three decades (Fig. 1). This impairs our ability to detect oxygen concentration changes in the ocean (Keeling et al. 2010). The number of oxygen profiles supplied by profiling floats nearly offsets the decrease in hydrocast data (Fig. 1), and this number is poised to increase even faster (Gruber et al. 2010). However, the optode calibration errors greatly reduce the suitability of the profiling float data for studies of long-term change.

Körtzinger et al. (2005) suggested that the optode, mounted on the upper endcap of a profiling float, could be recalibrated by measuring the partial pressure of oxygen in air. Subsequent research supports this idea, but most studies have focused on the results from one or a few floats (Emerson and Bushinsky 2014; Fiedler et al. 2013; Bittig and Körtzinger 2015). One essential conclusion from these studies is that there is no bias between sensor measurements in air or water. Here, we report on the efficiency of air calibration of Aanderaa oxygen sensors on an array of 47 profiling floats with some deployments over 5 years in length.

2. Sensor background

The Aanderaa optodes detect a change in fluorescence lifetime of a platinum porphyrin compound embedded in a gas-permeable foil (Klimant et al. 1997; Tengberg et al. 2006) to determine oxygen in water or air. The average fluorescent lifetimes of the lumiphores in the foil are quantified by measuring the phase shift in fluoresced red light relative to the modulated blue light excitation signal (Lippitsch et al. 1988). Fluorescence lifetime (τ) and phase shift (φ) are related [$\tau = \tan\varphi/(2\pi f)$] through the modulation frequency (f). The change in fluorescence lifetime is proportional to the partial pressure of oxygen at the sensing foil (Lippitsch et al. 1988; Bambot et al. 1994). In the presence of oxygen the fluorescence is quenched because the internal energy from the blue-light-excited lumiphore is dissipated by oxygen when the oxygen molecules collide with the lumiphore (dynamic quenching) (Lakowicz 2006). This shortens the fluorescence lifetime and reduces the phase angle difference between the excitation and fluorescent emission signals.

Dynamic quenching of fluorescence can be described within the framework of the Stern–Volmer model, which relates lifetime to oxygen concentration through the equation

$$\frac{\tau_0}{\tau} = 1 + k_q \tau_0 [\mathrm{O}_2], \tag{1}$$

where τ_0 is the unquenched (anoxic) lifetime, τ is the observed value, and $[\mathrm{O}_2]$ is the concentration (or partial pressure) of the quenching agent (oxygen). Term k_q is the bimolecular quenching constant, which is a measure of the quenching efficiency of oxygen as well as the ability of oxygen to contact the lumiphore (Lakowicz 2006). At higher oxygen concentrations, the Aanderaa optode response deviates from the Stern–Volmer model, which suggests that a fraction of the lumiphore is inaccessible to molecular oxygen (Lakowicz 2006). To compensate for this deviation, the Aanderaa sensors use a high-order polynomial to relate lifetime either to oxygen concentration or to the partial pressure of oxygen depending on the sensor model. Despite these complications, the Stern–Volmer model is useful for explaining our recalibration strategy.

Oxygen has a quenching efficiency close to unity, so changes in the quenching constant are likely due to changes in oxygen's accessibility to the lumiphore (Lakowicz 2006). Our hypothesis is that storage drift results when some of the lumiphore becomes inaccessible to oxygen quenching over time. This, in turn, decreases the overall quenching response of the lumiphore for a given partial pressure of oxygen. Leaching and bleaching should only

TABLE 1. Profiling float deployment information, gain values, percent air oxygen vs percent surface water oxygen saturation slopes, and long-term linear rates of change in percent air oxygen for floats assembled at UW. Filtered gain values were computed only when the absolute difference between percent air oxygen and surface water saturation was less than 2%. *WOA* gain values were determined following Takeshita et al. (2013). Confidence interval (CI) for the linear trend in percent air oxygen (% yr^{-1}) is 95%. The asterisk means insufficient data for this analysis; the term *ice* indicates a float deployed in ice-covered waters.

UW Float No.	WMO No.	Date deployed	Deployment position (Lat, lon)	Optode type	Gain (All data)	Gain (Filtered)	Gain (*WOA*)	Air vs water (Slope)	Air O_2 trend (% yr^{-1} ± CI)
6091	5904179	26 May 2014	60°S, 174°E	3830	1.131	1.133	1.130	0.18	*
6967	5903612	11 Dec 2011	42°S, 8°E	4330	1.070	1.073	1.074	0.22	−0.19 ± 0.14
6968	5903718	6 Mar 2012	50°S, 178°E	3830	1.162	1.163	1.155	0.22	−0.22 ± 0.11
7552	5903729	15 Mar 2012	44°S, 101°E	3830	1.135	1.135	1.134	0.21	0.12 ± 0.16
7557	5904181	28 Mar 2014	63°S, 184°E	4330	1.101	1.102	1.120	0.06	*
7558	5903711	25 Mar 2012	14°N, 236°E	4330	1.073	1.073	1.079	0.25	0.69 ± 0.59
7564	5903592	23 Aug 2011	76°N, 357°E	3830	1.084	1.083	1.074	0.17	Ice
7567	5904182	30 Mar 2014	66°S, 198°E	4330	1.087	1.085	*	*	Ice
7596	5903887	1 Aug 2012	75°N, 354°E	3830	1.163	1.168	1.138	0.14	Ice
7601	5903714	18 Feb 2012	50°N, 215°E	4330	1.098	1.102	1.107	0.29	0.36 ± 0.10
7613	5904180	31 Mar 2014	66°S, 204°E	3830	1.115	1.115	1.118	*	Ice
7614	5904183	1 Apr 2014	67°S, 210°E	4330	1.148	1.146	*	*	Ice
7619	5904105	2 Mar 2013	65°S, 150°E	4330	1.032	1.035	0.998	*	Ice
7620	5904104	3 Mar 2013	63°S, 149°E	3830	1.134	1.128	1.200	0.26	Ice
7647	5904021	18 Nov 2012	35°N, 237°E	4330	1.043	1.043	1.040	0.22	0.43 ± 0.22
8486	5904124	19 May 2013	23°N, 202°E	4330	1.062	1.062	1.083	0.21	−0.12 ± 0.22
8514	5904172	14 Sep 2013	23°N, 202°E	4330	1.066	1.073	1.086	0.07	*
9031	5904396	11 Apr 2014	55°S, 210°E	4330	1.200	1.201	1.197	0.23	*
9091	5904184	3 Apr 2014	64°S, 210°E	4330	0.978	0.990	0.980	0.24	Ice
9092	5904185	7 Apr 2014	60°S, 210°E	4330	0.972	0.973	0.965	0.13	Ice
9095	5904188	14 Apr 2014	50°S, 210°E	4330	1.170	1.170	1.158	0.40	*
9096	5904469	10 Dec 2014	54°S, 0°E	4330	0.994	0.988	0.985	*	*
9254	5904395	20 Apr 2014	40°S, 210°E	4330	1.176	1.176	1.182	0.55	*
9313	5904474	7 Dec 2014	45°S, 7°E	4330	1.030	1.029	1.030	*	*

affect fluorescence intensity since phase shift and lifetime are only a function of dynamic quenching produced by O_2 collisions (Lippitsch et al. 1988; Bambot et al. 1994). By rearranging Eq. (1), it can be seen that oxygen data can be corrected by adjusting k_q to yield the observed oxygen concentration at a given phase angle:

$$k_q[\mathrm{O}_2] = \left(\frac{1}{\tau} - \frac{1}{\tau_0}\right), \tag{2}$$

where k_q is temperature dependent and our correction process effectively assumes that the temperature dependence of the sensor remains unchanged as storage drift occurs. The value of τ_0 and its temperature dependence are also assumed to remain unchanged. These temperature dependencies are captured in the manufacturer's calibration.

3. Methods

Aanderaa oxygen optodes were deployed on the upper endcap of Teledyne Webb Research Apex profiling floats. Of all the floats, 24 were assembled at the University of Washington (UW) (Table 1) and 23 were assembled by Teledyne Webb and deployed by Argo Canada (Table 2). A 24th Argo Canada float (WMO 4901136) was not included in the analysis as the in-water oxygen, temperature, and salinity data were excessively noisy, indicating a CTD fault. The optodes were mounted on 10-cm-long stems, supplied by Teledyne Webb, to raise them about 20 cm above the float waterline. The 10-cm length keeps the oxygen sensor below the top of the CTD, which provides some mechanical protection. On the UW floats, there were 17 model 4330 optodes and 7 model 3830 optodes. The Argo Canada optodes were all model 3830s. All sensors used the standard response rate foil and the standard Aanderaa firmware. Calibrations were supplied by the manufacturer and no further calibration of the sensor was undertaken prior to deployment.

The profiling float firmware enabled the oxygen sensor to make air oxygen measurement during the telemetry phase of each surface operation. For the UW floats, normally only one air oxygen measurement was obtained per surfacing, but if surface operations were interrupted by failure of any key step, the surface operations restarted and an additional air oxygen measurement was made. As a result, there were occasionally up to five air oxygen measurements collected during the

TABLE 2. Profiling float deployment information, gain values, percent air oxygen vs percent surface water oxygen saturation slopes, and long-term linear rates of change in percent air oxygen for floats deployed by Argo Canada. *WOA* gain values were taken directly from the supplemental tables published by Takeshita et al. (2013). NR = not reported by Takeshita et al. (2013); the asterisk means insufficient data.

WMO No.	Date deployed	Deployment position (Lat, lon)	Gain (All data)	Gain (Filtered data)	Gain (*WOA*)	Air vs water (Slope)	Air O_2 trend (% yr^{-1} ± CI)
4900494	25 May 2004	60°N, 311°E	0.988	0.999	0.994	0.71	−0.29 ± 0.08
4900497	2 May 2004	44°N, 304°E	1.017	1.020	1.028	0.44	0.83 ± 0.08
4900523	27 Aug 2004	50°N, 212°E	1.029	1.029	1.057	0.13	−0.04 ± 0.06
4900627	22 Oct 2005	43°N, 302°E	0.989	0.992	1.000	0.27	0.10 ± 0.06
4900637	23 Feb 2005	47°N, 229°E	0.991	0.998	0.986	0.47	0.17 ± 0.05
4900869	5 Jul 2006	53°N, 215°E	1.032	1.038	1.033	0.23	0.41 ± 0.06
4900870	4 Oct 2006	56°N, 219°E	1.043	1.050	1.048	0.17	−0.37 ± 0.07
4900871	18 Jul 2006	50°N, 220°E	1.041	1.048	1.050	0.25	0.29 ± 0.04
4900872	19 Jul 2006	50°N, 221°E	1.042	1.055	1.047	0.26	0.02 ± 0.05
4900873	4 Aug 2006	38°N, 215°E	1.026	1.030	1.049	0.55	0.22 ± 0.02
4900874	5 Aug 2006	43°N, 222°E	1.052	1.056	1.067	0.26	0.40 ± 0.03
4900879	31 May 2006	60°N, 311°E	1.055	1.055	1.070	0.19	1.29 ± 0.05
4900880	30 May 2006	49°N, 311°E	1.078	1.087	1.087	0.20	−0.31 ± 0.47
4900881	12 Oct 2006	42°N, 299°E	1.053	1.052	1.052	0.32	0.46 ± 0.07
4900882	15 Oct 2006	43°N, 302°E	1.054	1.053	NR	0.26	0.99 ± 0.04
4900883	28 Nov 2006	43°N, 310°E	0.998	1.008	1.012	0.71	−0.90 ± 0.40
4901134	11 Feb 2010	49°N, 231°E	0.863	0.858	0.888	0.06	0.15 ± 0.56
4901135	8 Feb 2010	49°N, 222°E	0.858	0.852	0.871	0.33	0.14 ± 0.88
4901137	9 Jun 2010	49°N, 228°E	0.872	0.871	0.882	0.25	1.24 ± 0.38
4901139	19 Apr 2010	44°N, 302°E	0.904	0.908	0.912	0.23	−0.46 ± 0.33
4901140	3 May 2010	44°N, 304°E	0.902	0.900	0.904	0.03	−0.04 ± 0.18
4901141	18 May 2010	59°N, 310°E	0.840	0.841	0.834	0.36	*
4901142	17 May 2010	58°N, 309°E	0.832	0.837	0.833	0.40	1.13 ± 1.48

surface drift. The Argo Canada floats made from 1 to 21 oxygen measurements while at the surface over time periods that approached 1 day in some cases. There were no apparent systematic trends in the surface data within each surfacing, so only data in the first 2 h were utilized to ensure coherence with the in-water measurement. During the profile, oxygen measurements are made as the float rises from 1000 or 2000 m with a vertical resolution changing from 50 m at depth to every 5 m in the upper 100 m. The shallowest measurement in the water column was 7 m for the UW floats. The Argo Canada floats made their shallowest measurements in the water column at 4-m depth.

The atmospheric pressure at each location where a float surfaced was estimated from the NCEP–NCAR reanalyses 4-times daily dataset (Kalnay et al. 1996; NCEP 2015). Pressure values were linearly interpolated from the four surrounding NCEP grid points to the location and time that the float surfaced. Climatological surface oxygen percent saturation values were extracted from the monthly gridded data in the *World Ocean Atlas 2009* (Garcia et al. 2010; NCEI 2015). Surface percent saturation values were linearly interpolated from the four *WOA* grid points that surround each float profile and interpolated linearly to the yearday of the profile using the monthly *WOA* data values.

4. Calculations

The air oxygen values were used to correct the reported (raw) oxygen values $(O_2)_{raw}$ by applying only a gain correction (G):

$$(O_2)_{corr} = G \times (O_2)_{raw}, \tag{3}$$

where $(O_2)_{corr}$ is the corrected oxygen concentration. The gain factor g on each profile i was determined from the ratio of the expected partial pressure of oxygen in air (pO_2) to the partial pressure of oxygen in air measured by the optode ($pO_{2,optode}$):

$$g_i = pO_2/pO_{2,optode}, \tag{4}$$

where pO_2 was calculated from the NCEP estimate of atmospheric pressure (P_{NCEP}) at the location and time of each float surfacing, the contribution of water vapor (assuming 100% humidity at the observed temperature), and the mole fraction of oxygen in dry air as

$$pO_2 = (P_{NCEP} - p_{H_2O}) \times 0.209\,46. \tag{5}$$

The vapor pressure of water was calculated using the empirical equation found in the Aanderaa model 4330 operating manual,

$$p_{H_2O} = e^{[52.57-[6690.9/(t+273.15)]-4.681\times\ln(t+273.15)]}, \quad (6)$$

where t is the temperature (°C). The gain factors g_i were then averaged to obtain a single value of G that was applied to all of the data for each float.

The optode phase angle measurements were transmitted to shore along with the optode temperature. The calibration equations supplied with the model 3830 optodes convert phase angle to oxygen as a concentration, whether measurements are made in water or air. The phase measurements were converted to oxygen concentration using the standard equations supplied by the manufacturer for measurements made in the water column. The phase shift measured with blue excitation light (B_{Phase}) is corrected to a calibrated phase as

$$D_{\text{Phase}} = A + B \times B_{\text{Phase}}. \quad (7)$$

The coefficients A and B are supplied by the manufacturer. The concentration of oxygen (μmol L^{-1}) is computed as

$$(O_2)_{\text{raw}} = C_0 + C_1 \times D_{\text{Phase}} + C_2 \times D^2_{\text{Phase}} + C_3 \times D^3_{\text{Phase}} + C_4 \times D^4_{\text{Phase}}, \quad (8)$$

where C_0–C_4 are temperature-dependent coefficients that are computed from the calibration equations supplied by the manufacturer. Using phase measurements in air, the gain factor g_i for the model 3830 optode is then computed as

$$g_i = [(O_2)_{\text{soly}} \times (P_{\text{NCEP}} - pH_2O)]/[(1013.25 - pH_2O)/(O_2)_{\text{raw,air}}], \quad (9)$$

where $(O_2)_{\text{soly}}$ is the oxygen solubility (μmol L^{-1}) in pure water at an atmospheric pressure of 1013.25-mbar pressure (Garcia and Gordon 1992).

The model 4330 optode calibration equations yield oxygen partial pressure directly. The phase shift measured with blue light (T_{Phase}) is corrected to a calibrated phase as

$$\text{Cal}_{\text{Phase}} = A + B \times T_{\text{Phase}}. \quad (10)$$

The partial pressure of oxygen is then computed as

$$pO_{2,\text{optode}} = C_0 \times t^{m0} \times \text{Cal}^{n0}_{\text{Phase}} + C_1 \times t^{m1} \times \text{Cal}^{n1}_{\text{Phase}} + \cdots + C_{27} \times t^{m27} \times \text{Cal}^{n27}_{\text{Phase}}, \quad (11)$$

where the coefficients C_0–C_{27} and the exponents m_0–m_{27} and n_0–n_{27} are supplied in the sensor calibration data, along with the A and B values. The gain factor on each profile can then be computed directly from Eq. (4) and all values averaged to obtain the mean gain G. The concentration of oxygen in water is calculated from the model 4330 optode data as

$$(O_2)_{\text{raw}} = (O_2)_{\text{soly}} \times pO_{2,\text{optode}}/[(1013.25 - p_{H_2O}) \times 0.209\,46]. \quad (12)$$

5. Results and discussion

a. Gain versus offset

Our premise is that a simple multiplier to concentration is sufficient to correct the measured oxygen values. This is based on the assumption that storage drift occurs when an increasing percentage of the lumiphore becomes inaccessible to the ambient oxygen molecules. There are, however, several alternative approaches by which sensor oxygen values may be corrected. These include additive offsets to observed concentrations instead of a multiplicative gain factor. The adjustments may also be applied to the raw phase values or to the concentrations. The former would be equivalent to calculating new calibrated phase values [Eqs. (7) or (10)]. Before we consider the application of air oxygen corrections in detail, we examine the consistency of the observational data with respect to these other possible approaches to sensor correction.

We do not consider additive offset corrections to be appropriate based on laboratory observations (Bittig and Körtzinger 2015) that show consistent change in the response of optode sensors at high oxygen concentrations but little or no change in the response at near-zero oxygen concentrations. Additive offset corrections are also not consistent with data collected in strong oxygen minimum zones. We have deployed four profiling floats in the eastern tropical North Pacific, the Arabian Sea, and the Bay of Bengal. These regions all contain oxygen minimum zones, where the oxygen concentrations are expected to be zero in parts of the subsurface water column. Following the approach of Takeshita et al. (2013), the oxygen concentrations reported by these optodes appear to be in error by 10–40 μmol kg^{-1} near the sea surface when factory calibrations are used. However, the oxygen concentrations reported in the strong oxygen minimum zones show little error. All of these floats report oxygen concentrations between 0 and 1 μmol kg^{-1} in the core of the oxygen minimum. Complementary nitrate profiles reported by these floats often show significant reversals in concentration, indicative of nitrate consumption by denitrification or anaerobic ammonium oxidation. One example is shown by Takeshita et al. (2013) for float 7558

(corresponding WMO identification numbers for all UW floats are found in Table 1). These processes are inhibited at oxygen concentrations above the low nanomolar range (Dalsgaard et al. 2014). This supports the expectation that oxygen concentrations are essentially at zero in the core of these oxygen minimum zones and that the anoxic phase shift (τ_0) remains unchanged over time.

For such floats in strong oxygen minima, an offset correction to either reported concentration or phase angle that was of sufficient magnitude to correct surface oxygen values to the appropriate range would produce large errors within the core of the oxygen minimum. A multiplicative gain correction applied to concentration, however, can correct the surface concentrations and preserve the sensor accuracy at the near-zero concentrations found in the oxygen minimum. For these reasons, we have chosen to adjust oxygen concentrations using a gain correction [Eq. (3)] only.

The gain correction could be applied directly to concentrations, or it could be applied to the phase measurements. We discuss this further in section 5d, where we report that moderately better agreement with the Winkler titration measurements made on the deployment cruises is found when the gain correction is applied directly to concentration as in Eq. (3). We therefore have used this approach throughout the paper.

b. *Air oxygen values*

The oxygen sensors on our profiling floats are only about 20 cm above the waterline and likely to be subject to considerable interaction with the surface ocean. It is essential to understand to what degree the oxygen measurements made while the float is at the surface are responding to the partial pressure of oxygen in the air, rather than surface water oxygen values. It is not possible for a profiling float to communicate or to obtain a position fix while it is submerged. Since communication and geolocation do occur, the oxygen measurements made while the float is at the surface must, to a large extent, occur in air. The air oxygen measurements may still be biased by spray or overwash by waves. To assess the influence of seawater on the air oxygen measurements, we first consider the time series of surface water oxygen and air oxygen that have been collected by float 7601 (Table 1), which was deployed at Ocean Station Papa (OSP; 50°N, 145°W) in the North Pacific.

Figure 2 shows a 3-yr record of percent saturation for oxygen near OSP. The float estimates of percent saturation for surface seawater [$100 \times (O_2)_{raw}/(O_2)_{soly,NCEP}$] and air ($100 \times pO_{2,optode}/pO_2$) are scaled on the left axis and are compared to interpolated *WOA* 2009 values scaled on the right axis. The float estimates were calculated using the factory calibration, with its inherent

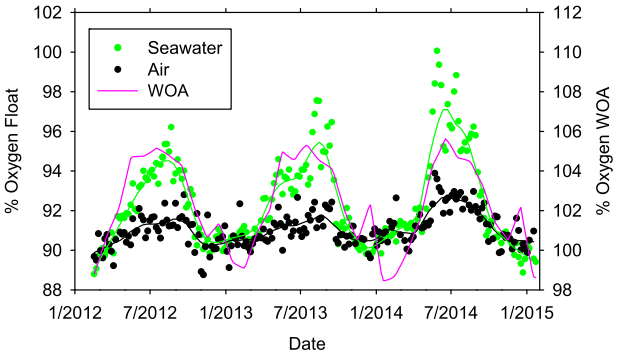

FIG. 2. Percent of expected air oxygen partial pressure measured by the optode (black dots), and percent of surface water oxygen saturation reported by the sensor (green dots) vs time for float 7601. The cyan line is the climatological value of percent surface oxygen saturation at the location and year fraction of each float profile that was obtained from the *World Ocean Atlas 2009* (Garcia et al. 2010).

uncertainty. Term $(O_2)_{soly,NCEP}$ is the oxygen solubility at the measured surface temperature and salinity values using the NCEP estimate for atmospheric pressure. The NCEP atmospheric pressure, which was used to compute surface water oxygen solubility, is the mean of the prior one month of values at each surfacing of a float, rather than the canonical atmospheric pressure of 1013.25 mbar. The oxygen reequilibration time with the atmosphere tends to be in the range of a week to near one month in open ocean waters (Broecker and Peng 1974; Luz and Barkan 2000), and the atmospheric pressure can deviate significantly from 1013.25 mbar over monthly time scales. The oxygen saturation will reflect the mean surface atmospheric pressure over this time, so we use the observed value averaged over the previous one month of profiles.

The data in Fig. 2 show a clear annual cycle in surface water percent saturation and a weaker annual cycle in the percent of air oxygen reported by the optode. The percent air oxygen values are significantly correlated to the surface water percent saturation reported by the optode, with a slope of 0.29 (Fig. 3). During periods when the *WOA* climatology indicates that the surface water oxygen concentrations are near equilibrium with the atmosphere, the air and surface water percent saturation values reported by the optode on float 7601 are quite similar to each other (Fig. 2). A relationship comparable to that in Fig. 3 was first reported by Bittig and Körtzinger (2015). The linear correlation between percent air oxygen detected by the sensor and surface water percent saturation was seen for all of the UW optodes (Table 1), with a mean slope of 0.22 ± 0.12 (1σ). The mean value for the Argo Canada floats (Table 2) was 0.31 ± 0.18. Several of the Argo Canada floats have

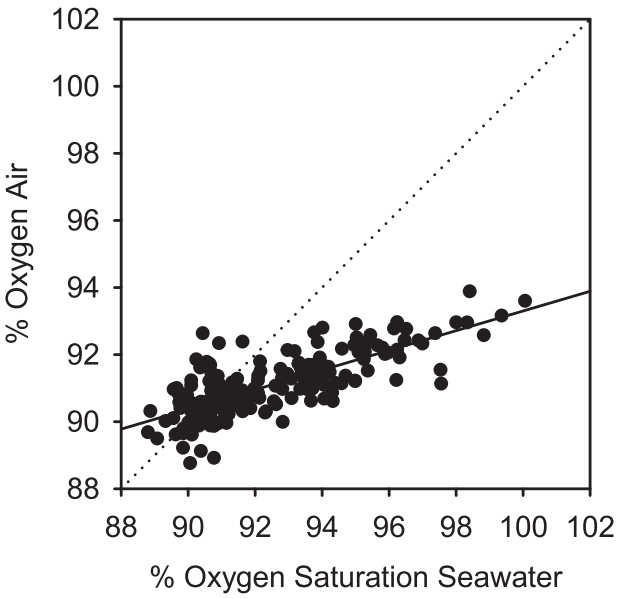

FIG. 3. Percent of the expected air oxygen partial pressure vs percent saturation of surface water reported by float 7601. Dotted line is a 1:1 relation, and solid line is a least squares fit with slope 0.29 using a model I regression.

relatively higher slopes, up to 0.7 (Table 2). The high values are not clearly related to high latitudes and stormy conditions that might produce more interaction of water with the sensor during air measurements. The high slope may result if a float has low positive buoyancy at the surface.

The percent air oxygen values should be nearly constant, varying only with atmospheric pressure. A linear relationship between percent air oxygen and surface water percent oxygen saturation with a mean slope of 0.27 ± 0.16 (all floats) suggests that the optode air oxygen measurement is responding to a mix of about 75% air and 25% water. Determination of the gain factor G using all of the air oxygen measurements would include some bias from seawater. This bias in G can be high when seawater is supersaturated with oxygen during high primary production, or low when deep mixing brings oxygen-depleted water to the surface. In this paper, we consider two approaches for the computation of G. One is to compute G using the mean of all air oxygen measurements reported by a float. In this case, if surface water averaged 3% supersaturated, then the value of G might be biased high by $0.25 \times 3\% = 0.75\%$. Average oxygen supersaturation is generally less than 3% for most of the year at any location and the bias is thus probably somewhat less than 0.75%. A second approach is to compute G using air oxygen measurements made only when the surface water and air oxygen values differ by less than 2% saturation. In this case, the influence of surface water on the air oxygen value should produce a bias on the order of 0.5% ($0.25 \times 2\%$) or less. Bittig and Körtzinger (2015) propose a third option, which involves the correction of all air oxygen observations for surface water contamination to yield values at a reference state where the air and water percent saturation is the same. This requires using the mean slope from a plot similar to Fig. 3 for each float. This should produce results nearly equal to our second approach, where we have selected only air oxygen observations where the air and surface water percent saturation values are similar.

The values of G determined from all air oxygen measurements and the values that are filtered by selecting only measurements when the surface water and air oxygen values differ by less than 2% are shown in Table 1. There is negligible difference in the gain factor computed by the two methods, as long as the data record spans a full year or more.

c. *Oxygen sensor stability over time*

Thus far, we have considered only the use of a mean gain factor that is determined over the life of a float. However, if the sensor is not stable in time, an appropriate strategy might be to update the gain factor more frequently, to correct for temporal drift. Air oxygen concentrations represent a stable source against which the magnitude of sensor drift can be assessed (Körtzinger et al. 2005; Bittig and Körtzinger 2015), providing that atmospheric pressure can be estimated accurately at the float location.

Of the floats used, 29 of them and their oxygen sensors have now operated for more than 1 yr in ice-free waters, and these records are suitable for analysis of systematic temporal change in the air oxygen values. We do not consider the long-term records for floats in ice-covered regions because these floats make no air measurement in winter and relatively few air oxygen measurements in summer. Figure 4 shows multiyear records of percent air oxygen determined from optode sensors for four UW floats and four Argo Canada floats that were deployed in a variety of environments. The long-term change in percent air oxygen was derived from a deseasonalized linear regression of the percent air oxygen values,

$$100 \times \mathrm{pO}_{2,\mathrm{optode}}/\mathrm{pO}_2 = a + b \times \sin(2 \times \pi \times D/365.25) + c \times \cos(2 \times \pi \times D/365.25) + d \times D. \quad (13)$$

The values of a–d are fitted regression coefficients, where b and c determine a mean annual cycle; and D is the elapsed time in days. The linear coefficient d is on the order of a few tenths of a percent per year in most cases (Fig. 5).

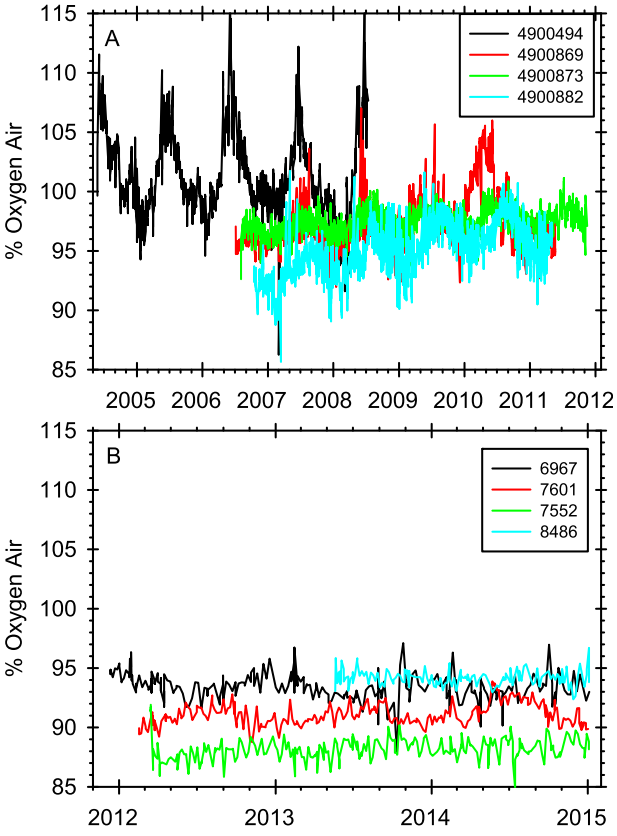

FIG. 4. Percent of the expected air oxygen partial pressure reported by float sensors vs time. (a) Argo Canada floats. (b) UW floats. Deployment locations are found in Tables 1 and 2. All measurements on each surfacing are shown.

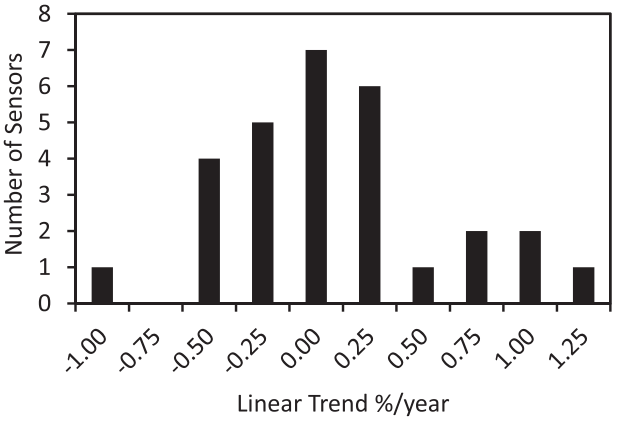

FIG. 5. Histogram of linear trend rates (d) determined from least squares fit of the percent of air oxygen observed with UW/MBARI and Argo Canada float oxygen sensors to Eq. (13).

Both positive and negative values of the linear trend term d are observed (Tables 1 and 2), and the mean of all values ($0.2\%\,\mathrm{yr}^{-1}$) is not significantly different from zero. It is generally believed that drift in the optode sensor only occurs toward lower oxygen concentrations (negative d) (D'Asaro and McNeil 2013; Bittig and Körtzinger 2015). The occurrence of both positive and negative linear trends suggests that storage drift is not the main driver of these changes in air oxygen detected by the optode sensors. The annual cycle that is seen in most records makes it clear that surface water has a significant effect on the air oxygen measurement. In several cases, the large positive and negative drift rates appear to be produced by large interannual variability in the annual cycle (e.g., float 4900869; Fig. 4a), which produces large residuals when a constant annual cycle is removed from the data. This may occur as floats drift through large gradients in net community production. Uncertainty in the NCEP atmospheric pressure may also influence the linear drift rates (Hines et al. 2000). A comparison of NCEP sea level atmospheric pressure to values observed on research vessels has a root-mean-square (RMS) error of 2.7 hPa, with RMS biases up to 7 hPa at high latitudes (Smith et al. 2001). Errors of this magnitude could account for nearly the entire linear drift rate, but only if they varied systematically in time.

Given that the linear trends in percent air oxygen are generally small, at only a few tenths of a percent per year and with a mean near zero, of both positive and negative amplitude, and of the magnitude where surface water contamination can have a significant influence, we have concluded that there is not yet a reason to assume that the sensors are drifting. This is consistent with the assessment of Takeshita et al. (2013). We have used only a single gain correction determined from all of the available data to correct the oxygen data for each float.

The dominant source of variability in the air oxygen measurements was the interaction with surface water, probably due to some wave overwash. The contamination by surface water produces the distinct annual cycle in air oxygen shown in Figs. 2 and 4. This variability was much greater than the variability measured within a single surfacing by the Argo Canada floats, where as many as 21 air oxygen values were measured each time a float surfaced. There was, therefore, little benefit to be obtained by making multiple air oxygen measurements on a single float surfacing, when the surface values from many profiles are averaged to obtain a mean value for G. For example, float 4900494, whose air oxygen percent saturation values are shown in Fig. 4a, made an average of 13 air measurements on each surfacing. The mean air oxygen is 101.4% of the expected value whether computed using all of the data from each surfacing or just the first observation made on each surfacing. The extra 12 air oxygen measurements on each surfacing do not improve the estimate of G.

d. Comparison to Winkler titrations

High-quality Winkler titration data were collected at 11 of the stations where UW floats were deployed. It should be noted that the Winkler titrations are never made on samples collected simultaneously with the float profile. Our floats are generally deployed when the ship leaves the station to avoid any possible damage if a float surfaces under the ship. About 18 h then elapse before the float resurfaces with measurements made during the last 2–4 h of that period. An additional lag between the observations made on board the ship and by the float may occur for deployments at time series stations that span several days. Sample collection for oxygen titration is seldom the last task, and an additional time offset generally occurs between the two datasets. Estimating the effect of these lags is difficult because there are generally no high-frequency data available that would allow the possible error size to be estimated. Data that have been reported for moored oxygen sensors in the open ocean show that rapid changes of 5–10 μmol O_2 kg^{-1} in a day occur frequently (Emerson et al. 2008; Martz et al. 2014; Weeding and Trull 2014). An exact correspondence between the profiling float data and Winkler data is not to be expected. These errors should be random and have a mean near zero for a large number of floats.

Figure 6 shows a comparison of the gain-corrected profiling float oxygen measurements versus Winkler titrations made at the same depths for floats deployed at Ocean Station *Papa* in the North Pacific (7601), the Hawaii Ocean Time Series station in the subtropical Pacific (8486), and four floats in the Southern Ocean (9254, 9095, 9092, and 9091). This comparison includes floats deployed in the subtropics at surface temperatures near 25°C and floats in the Southern Ocean with surface temperatures of −1°C.

The mean difference between Winkler oxygen values and the air gain-corrected values reported by the floats in the mixed layer was 2.4 ± 5.7 (1σ, $N = 30$) μmol kg^{-1}. The mean difference is not significantly different from zero ($p < 0.01$). The scatter in the differences, as encapsulated by the standard deviation, is larger than might be expected. This must reflect, in part, the time differences between when Winkler samples were collected and the floats surface, as well as the inherent uncertainty in calibrating Winkler titrations and the float sensors, as we note above. Several of the floats with Winkler calibrations were also deployed in ice-covered waters. There are relatively few air oxygen measurements for these floats, which adds more uncertainty to their air calibrations. Eliminating these floats reduces the mean difference and standard deviation to 2.1 ± 4.5 μmol kg^{-1}.

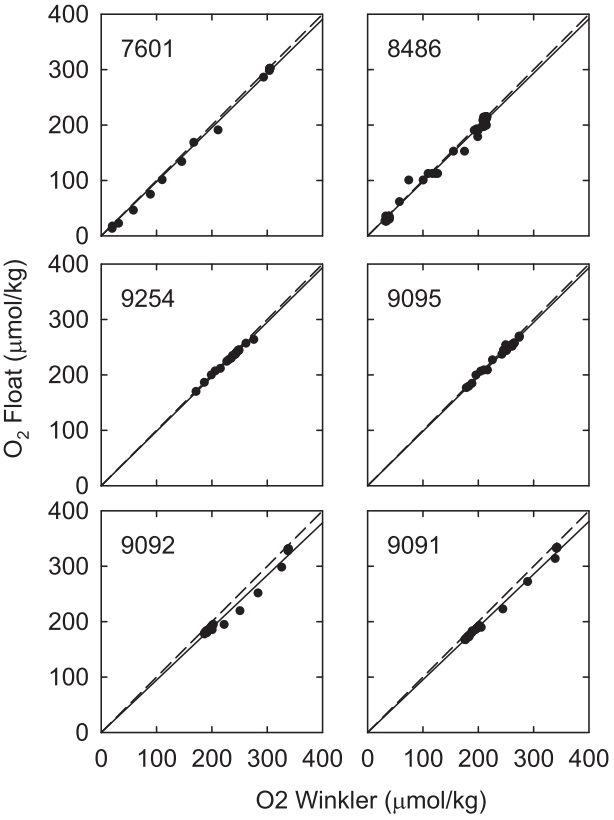

FIG. 6. Gain-corrected oxygen concentrations computed from float sensor observations vs Winkler oxygen titration values at matched depths. The first float profile was used in each case except for float 7601. Profile 1 for that float exhibited a considerably different density structure than seen on the bottle cast, so profile 2 was used. Dashed lines are a 1:1 relationship, and solid black lines are least squares fits forced through the 0,0 intercept.

The relative uncertainty from the mean error in the surface ocean oxygen values for the array of floats that received Winkler calibrations appears to be less than 1% (2.1 relative to about 250 μmol kg^{-1}). In contrast, the mean relative error of the uncorrected oxygen sensor data in the mixed layer from the floats is 10%. Air calibration has thus improved the accuracy of the oxygen sensor array by about a factor of 10.

The mean difference of the sensor data from Winkler values for all samples from the entire water column sampled by the floats ($N = 269$) was somewhat larger than in the mixed layer (6.7 ± 7.6 μmol kg^{-1}). Values were matched on the basis of depth, and the variability will reflect the additional uncertainty caused by vertical motions of isopycnal surfaces. The largest residuals (Winkler minus float) are skewed in the positive direction, which likely also reflects the effect of dynamic errors created by the somewhat slow response rate of the sensor (Bittig et al. 2014). The sensor values in the oxycline reported by floats 9092 and 9091 are notable for

the extent to which they fall below the 1:1 line for a comparison to Winkler titration values (Fig. 6). These floats were deployed in water with subzero temperatures. Sensor response rates would be at their slowest (Bittig et al. 2014). The offset for floats 9092 and 9091 may also reflect the very low temperature of the water in which these floats profiled, which lies outside the temperature range at which they were calibrated. Dynamic errors can be mitigated by pumping the sensor (Bittig et al. 2014), but this would complicate the potential for air calibrations.

We have also computed a gain correction for the phase angle measurements that adjusts the air oxygen values to yield the proper pO_2 while constraining the phase angle that yields zero oxygen to be unchanged. Because the phase angle at zero oxygen is not zero, this requires a slope and offset adjustment to the phase angle. The slope and offset values for the phase angle were computed from the two constraints: 1) the phase angle that yields zero oxygen be unchanged when transformed by the slope and offset and 2) the transformed phase angle in air must yield the correct partial pressure of oxygen. The slope and intercept values for each profile were then averaged, and the mean values were used to transform the observed phase angles on each profile. Oxygen concentration was subsequently computed with the transformed phase angles. This transformation yields no substantial difference from the oxygen values corrected with a gain factor applied to concentration near the surface or in oxygen-deficient regions. At oxygen concentrations near 50% saturation, the two methods of correction yield oxygen concentrations that may differ by about $4\,\mu\text{mol kg}^{-1}$. In almost all cases where we have Winkler data, the application of a gain correction to concentration, rather than to phase angle, yields moderately better agreement between the float data and the titrations. This implies that the storage drift effect is primarily influencing the k_q term in Eq. (1), rather than the phase angle itself. The difference between the two approaches to correcting oxygen was not statistically significant, however. Because the computation of a gain factor in concentration is much simpler, we have adopted that approach.

e. *Comparison to Takeshita et al. (2013)*

Winkler titrations are not available for most float deployments. The gain factors that we determined from air oxygen for all of the floats were therefore compared to the gain corrections determined by the methods outlined in Takeshita et al. (2013). Takeshita et al. (2013) report several possible correction methods. We utilize the gain-only correction, which is based on correcting the mean percent saturation of surface water determined with the uncorrected sensor calibration to match the mean percent saturation values in the *World Ocean Atlas 2009* (Garcia et al. 2010) climatology at the same position and yearday of each float profile. This yields a gain correction term that is comparable to our G value determined from air oxygen measurements.

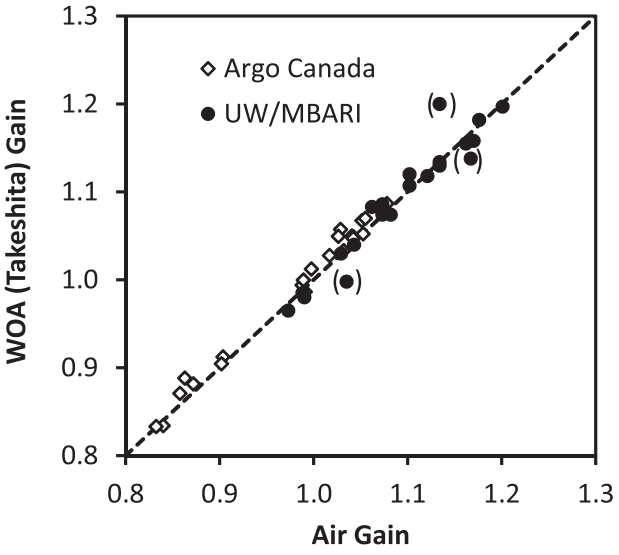

FIG. 7. Float sensor gain determined by comparison to *World Ocean Atlas 2009* surface oxygen percent saturation (Takeshita et al. 2013) vs the air oxygen gain computed using all data. UW/MBARI values in parenthesis are in marginal ice zones, where there is substantial uncertainty in the *WOA* values. Dashed line is a 1:1 relationship.

The comparison of the two correction terms is shown in Fig. 7. The least squares line fitted through all the data is indistinguishable from a 1:1 line ($p < 0.05$). The standard error of estimate for a regression line fitted to the data in Fig. 7 is 0.016, or a 1.6% uncertainty in the *WOA* gain factor, relative to the gain factor determined from air oxygen. Further, the three largest residuals are from floats in ice-covered waters, where there is large uncertainty in the *WOA* values. If these values are eliminated, then the standard error of estimate is reduced to 0.010, or a 1% uncertainty when comparing the two gain factors.

We note that these two correction schemes are completely independent. Takeshita et al. (2013) is based on comparing surface water oxygen saturation values to the *World Ocean Atlas 2009* climatology. Our correction is based on comparing air oxygen partial pressures to the expected values based on the NCEP air pressure. The agreement is an independent confirmation that a robust correction to float oxygen data can be determined from air oxygen or a comparison to the surface water oxygen climatology in most locations (ice-covered waters being an exception). Where air oxygen values were not measured, the methods described by Takeshita et al. (2013)

can be applied with high confidence. It is, therefore, possible to substantially improve the accuracy of the raw oxygen data reported by Argo floats, which now exceed greatly the number of profiles reported each year by shipboard titrations (Fig. 1).

There is good agreement (<1% difference) between the air gain factors and the *WOA* gain factors (Table 2) even for floats such as 4900494, which have extremely large annual cycles in the percent air oxygen values (Fig. 4a). The large summer air oxygen values are driven by the overwash of supersaturated surface waters with high primary production. This effect must be offset over the annual average by air gain values that are too low in winter when the sensor is influenced by surface waters that are undersaturated with oxygen as deeper mixing occurs. The biases in the percent air oxygen values that are driven by these processes must nearly cancel over an annual cycle.

Argo Canada floats that were deployed from 2004 to 2006 (Table 2) all used a model 3830 sensor with the internal reference salinity set to 35, whereas those deployed in 2010 have a salinity setting of 0. The 2004–06 floats have gains near 1 to 1.1, consistent with the UW and Monterey Bay Aquarium Research Institute (MBARI) sensors and with a storage drift toward lower sensitivity. The 2010 floats are almost unique in the dataset analyzed by Takeshita et al. (2013), with sensor gains systematically lower than 1 (Fig. 7; Table 2). This indicates greater sensitivity to oxygen than expected from the factory calibration, and is inconsistent with storage drift to lower oxygen sensitivity. Such a result would occur if the software used to process the in-water data presumed that the internal salinity had been set to 35, as had the earlier sensors, rather than 0. The gain correction reported here would correct such an error.

6. Conclusions

It is clear from our observations that air oxygen measurements can be used to substantially improve the performance of optode oxygen sensors on profiling floats. The overall accuracy of the sensor array is better than 1% near the surface when a gain factor, derived from air oxygen measurements, is applied to the oxygen concentration measurements. The air oxygen measurements also show a linear trend in time of a few tenths of a percent, with both positive and negative values. The linear trend is distinct from storage drift, which occurs only in the negative direction. It is, therefore, likely that the linear trend in air oxygen measurements represents biases such as variable influence of surface water on the air measurement, rather than sensor drift. It may not be a reflection of a temporally changing error in surface water oxygen values.

Air oxygen measurements should be a standard protocol on all autonomous platforms, such as profiling floats, that periodically reach the ocean surface. It may be possible to apply this calibration to glider measurements as well, but it would require reconfiguring installations that typically have the optodes on the underside of the glider. If air oxygen measurements are not available, then the results in Fig. 7 show that the procedures described by Takeshita et al. (2013) can also be used to correct oxygen sensor values with an uncertainty near 1% at the surface. The air oxygen method of correction is preferable, however, because it is entirely independent of the ocean oxygen climatology.

The current uncertainty in Winkler oxygen measurements that can be assessed from large scale ocean surveys is also on the order of 1%. For example, the error in dissolved oxygen concentration was 1.6% in the Carbon Dioxide in the Atlantic Ocean (CARINA) dataset before crossover adjustments were made (Tanhua et al. 2010). It is, therefore, conceivable that a network of profiling floats equipped with oxygen sensors, and that makes air oxygen calibration measurements, can produce data that rival the consistency of that found in large international ocean surveys using Winkler titrations. The number of oxygen measurements being made by profiling floats in open ocean waters now greatly surpasses the number of Winkler titrations that are being made from ships (Fig. 1). The application of air oxygen calibration to this array should enable a vastly improved system for detection of oxygen change in the open ocean.

Our recommended procedure for determining air oxygen is as follows:

1) The oxygen sensor should be mounted on a stem at least 10 cm long to raise the sensor above the waterline. Longer stems are probably beneficial in terms of minimizing the impact of surface water on the air oxygen measurement, but that benefit must be traded with the risk of exposing the sensor to damage during launch or environmental conditions at the sea surface.
2) Each float should make one air oxygen measurement (including sensor temperature) at the surface during each float cycle. Additional measurements have little impact on the air gain value. However, there is little penalty in power or data transmission costs if more measurements are made.
3) The air pressure estimate used to compute the air oxygen percent saturation on each profile and associated metadata for the air pressure estimate should be recorded along with adjusted data in the delayed mode files.

4) At least one year of data should be used to compute the sensor gain factor.

Acknowledgments. This work was supported by the David and Lucile Packard Foundation; the Southern Ocean Carbon and Climate Observations and Modeling (SOCCOM) program through the National Science Foundation's Office of Polar Programs Grant PLR-1425989 and NSF Grant 0825348; National Oceanographic Partnership Program Grant N00014 09 10052; and NOAA Grant NA17RJ1232, part 2, to the University of Washington and to the Department of Fisheries and Oceans Canada. Dana Swift, Dale Ripley, and Rick Rupan at the University of Washington, and Luke Coletti, Hans Jannasch, and Carole Sakamoto at MBARI contributed immensely to this work. Anh Tran decoded the surface drift phase oxygen data for the Argo Canada floats. We gratefully acknowledge the Hawaii Ocean Time Series program, the Line P Program at the Institute of Ocean Sciences (Canadian Department of Fisheries and Oceans), and the GO-SHIP P16S cruise (Lynne Talley, chief scientist) for deploying floats and providing rapid, online access to their data. Henry Bittig and two anonymous reviewers provided helpful comments and corrections that improved the manuscript.

REFERENCES

Bambot, S. B., R. Holavanahali, J. R. Lakowicz, G. M. Carter, and G. Rao, 1994: Phase fluorometric sterilizable optical oxygen sensor. *Biotechnol. Bioeng.*, **43**, 1139–1145, doi:10.1002/bit.260431119.

Bittig, H., and A. Körtzinger, 2015: Tackling oxygen optode drift: Near-surface and in-air oxygen optode measurements on a float provide an accurate in situ reference. *J. Atmos. Oceanic Technol.*, **32**, 1536–1543, doi:10.1175/JTECH-D-14-00162.1.

——, B. Fiedler, R. Scholz, G. Krahmann, and A. Körtzinger, 2014: Time response of oxygen optodes on profiling platforms and its dependence on flow speed and temperature. *Limnol. Oceanogr.: Methods*, **12**, 617–636, doi:10.4319/lom.2014.12.617.

Boyer, T. P., and Coauthors, 2013: *World Ocean Database 2013.* S. Levitus and A. Mishonov, Eds., NOAA Atlas NESDIS 72, 209 pp., doi:10.7289/V5NZ85MT.

Broecker, W. S., and T. H. Peng, 1974: Gas exchange rates between air and sea. *Tellus*, **26A**, 21–35, doi:10.1111/j.2153-3490.1974.tb01948.x.

Czeschel, R., L. Stramma, and G. C. Johnson, 2012: Oxygen decreases and variability in the eastern equatorial Pacific. *J. Geophys. Res.*, **117**, C11019, doi:10.1029/2012JC008043.

Dalsgaard, T., F. J. Stewart, B. Thamdrup, L. De Brabandere, N. P. Revsbech, O. Ulloa, D. E. Canfield, and E. F. DeLong, 2014: Oxygen at nanomolar levels reversibly suppresses process rates and gene expression in anammox and denitrification in the oxygen minimum zone off northern Chile. *MBio*, **5**, e01966-e14, doi:10.1128/mBio.01966-14.

D'Asaro, E. A., and C. McNeil, 2013: Calibration and stability of oxygen sensors on autonomous floats. *J. Atmos. Oceanic Technol.*, **30**, 1896–1906, doi:10.1175/JTECH-D-12-00222.1.

Emerson, S., and S. Bushinsky, 2014: Oxygen concentrations and biological fluxes in the open ocean. *Oceanography*, **27**, 168–171, doi:10.5670/oceanog.2014.20.

——, C. Stump, and D. Nicholson, 2008: Net biological oxygen production in the ocean: Remote in situ measurements of O_2 and N_2 in surface waters. *Global Biogeochem. Cycles*, **22**, GB3023, doi:10.1029/2007GB003095.

Fiedler, B., P. Fietzek, N. Vieira, P. Silva, H. C. Bittig, and A. Körtzinger, 2013: In situ CO_2 and O_2 measurements on a profiling float. *J. Atmos. Oceanic Technol.*, **30**, 112–126, doi:10.1175/JTECH-D-12-00043.1.

Garcia, H. E., and L. I. Gordon, 1992: Oxygen solubility in seawater: Better fitting equations. *Limnol. Oceanogr.*, **37**, 1307–1312, doi:10.4319/lo.1992.37.6.1307.

——, R. A. Locarnini, T. P. Boyer, J. I. Antonov, O. K. Baranova, M. M. Zweng, and D. R. Johnson, 2010: *Dissolved Oxygen, Apparent Oxygen Utilization, and Oxygen Saturation.* Vol. 3, *World Ocean Atlas 2009*, NOAA Atlas NESDIS 70, 28 pp.

Gruber, N., and Coauthors, 2010: Adding oxygen to Argo: Developing a global in situ observatory for ocean deoxygenation and biogeochemistry. *Proceedings of OceanObs'09: Sustained Ocean Observations and Information for Society*, J. Hall, D. E. Harrison, and D. Stammer, Eds., Vol. 2, ESA Publ. WPP-306, doi:10.5270/OceanObs09.cwp.39.

Hines, K. M., D. H. Bromwich, and G. J. Marshall, 2000: Artificial surface pressure trends in the NCEP–NCAR reanalysis over the Southern Ocean and Antarctica. *J. Climate*, **13**, 3940–3952, doi:10.1175/1520-0442(2000)013<3940:ASPTIT>2.0.CO;2.

Johnson, K. S., S. C. Riser, and D. M. Karl, 2010: Nitrate supply from deep to near-surface waters of the North Pacific subtropical gyre. *Nature*, **465**, 1062–1065, doi:10.1038/nature09170.

Kalnay, E. M., and Coauthors, 1996: The NCEP/NCAR 40-Year Reanalysis Project. *Bull. Amer. Meteor. Soc.*, **77**, 437–470, doi:10.1175/1520-0477(1996)077<0437:TNYRP>2.0.CO;2.

Keeling, R. F., A. Körtzinger, and N. Gruber, 2010: Ocean deoxygenation in a warming world. *Annu. Rev. Mar. Sci.*, **2**, 199–229, doi:10.1146/annurev.marine.010908.163855.

Kihm, C., and A. Körtzinger, 2010: Air-sea gas transfer velocity for oxygen derived from float data. *J. Geophys. Res.*, **115**, C12003, doi:10.1029/2009JC006077.

Klimant, I., M. Kühl, R. N. Glud, and G. Holst, 1997: Optical measurement of oxygen and temperature in microscale: Strategies and biological applications. *Sens. Actuators*, **38B**, 29–37, doi:10.1016/S0925-4005(97)80168-2.

Körtzinger, A., J. Schimanski, U. Send, and D. Wallace, 2004: The ocean takes a deep breath. *Science*, **306**, 1337, doi:10.1126/science.1102557.

——, ——, and ——, 2005: High-quality oxygen measurements from profiling floats: A promising new technique. *J. Atmos. Oceanic Technol.*, **22**, 302–308, doi:10.1175/JTECH1701.1.

Lakowicz, J. R., 2006: *Principles of Fluorescence Spectroscopy.* 3rd ed. Springer, 954 pp.

Lippitsch, M. E., J. Pusterhoffer, M. J. P. Leiner, and O. S. Wolfbeis, 1988: Fibre-optic oxygen sensor with the fluorescence decay time as the information carrier. *Anal. Chim. Acta*, **205**, 1–6, doi:10.1016/S0003-2670(00)82310-7.

Luz, B., and E. Barkan, 2000: Assessment of oceanic productivity with the triple-isotope composition of dissolved oxygen. *Science*, **288**, 2028–2031, doi:10.1126/science.288.5473.2028.

Martz, T. R., K. S. Johnson, and S. C. Riser, 2008: Ocean metabolism observed with oxygen sensors on profiling floats in the

Pacific. *Limnol. Oceanogr.*, **53**, 2094–2111, doi:10.4319/lo.2008.53.5_part_2.2094.

——, U. Send, M. D. Ohman, Y. Takeshita, P. Breshahan, H.-J. Kim, and S. Nam, 2014: Dynamic variability of biogeochemical ratios in the Southern California Current System. *Geophys. Res. Lett.*, **41**, 2496–2501, doi:10.1002/2014GL059332.

NCEI, 2015: *World Ocean Atlas 2009*. National Centers for Environmental Information, accessed 3 August 2015. [Available online at http://www.nodc.noaa.gov/OC5/WOA09/pr_woa09.html.]

NCEP, 2015: NCEP/NCAR Reanalysis 1. National Centers for Environmental Prediction, accessed 2 April 2015. [Available online at http://www.esrl.noaa.gov/psd/data/gridded/data.ncep.reanalysis.html.]

Prakash, S., T. M. B. Nair, T. V. S. U. Bhaskar, P. Prakash, and D. Gilbert, 2012: Oxycline variability in the central Arabian Sea: An Argo-oxygen study. *J. Sea Res.*, **71**, 1–8, doi:10.1016/j.seares.2012.03.003.

Riser, S. C., and K. S. Johnson, 2008: Net production of oxygen in the subtropical ocean. *Nature*, **451**, 323–325, doi:10.1038/nature06441.

Smith, S. R., D. M. Legler, and K. V. Verzone, 2001: Quantifying uncertainties in NCEP reanalyses using high-quality research vessel observations. *J. Climate*, **14**, 4062–4072, doi:10.1175/1520-0442(2001)014<4062:QUINRU>2.0.CO;2.

Takeshita, Y., T. R. Martz, K. S. Johnson, J. N. Plant, D. Gilbert, S. C. Riser, C. Neill, and B. Tilbrook, 2013: A climatology-based quality control procedure for profiling float oxygen data. *J. Geophys. Res. Oceans*, **118**, 5640–5650, doi:10.1002/jgrc.20399.

Tanhua, T., S. van Heuven, R. M. Key, A. Velo, A. Olsen, and C. Schirnick, 2010: Quality control procedures and methods of the CARINA database. *Earth Syst. Sci. Data*, **2**, 35–49, doi:10.5194/essd-2-35-2010.

Tengberg, A., and Coauthors, 2006: Evaluation of a lifetime-based optode to measure oxygen in aquatic systems. *Limnol. Oceanogr. Methods*, **4**, 7–17, doi:10.4319/lom.2006.4.7.

Thomson, R. E., T. A. Curran, M. C. Hamilton, and R. McFarlane, 1988: Time series measurements from a moored fluorescence-based dissolved oxygen sensor. *J. Atmos. Oceanic Technol.*, **5**, 614–624, doi:10.1175/1520-0426(1988)005<0614:TSMFAM>2.0.CO;2.

Uchida, H., T. Kawano, I. Kaneko, and M. Fukasawa, 2008: In situ calibration of optode-based oxygen sensors. *J. Atmos. Oceanic Technol.*, **25**, 2271–2281, doi:10.1175/2008JTECHO549.1.

Ulloa, O., D. E. Canfield, E. F. DeLong, R. M. Letelier, and F. J. Stewart, 2012: Microbial oceanography of anoxic oxygen minimum zones. *Proc. Natl. Acad. Sci. USA*, **109**, 15 996–16 003, doi:10.1073/pnas.1205009109.

Weeding, B., and T. W. Trull, 2014: Hourly oxygen and total gas tension measurements at the Southern Ocean Time Series site reveal winter ventilation and spring net community production. *J. Geophys. Res. Oceans*, **119**, 348–358, doi:10.1002/2013JC009302.